Applied Catalysis B: Environmental 97 (2010) 28–35

Contents lists available at ScienceDirect

Applied Catalysis B: Environmental

journal homepage: www.elsevier.com/locate/apcatb

Preferential oxidation of carbon monoxide on Co/CeO_2 nanoparticles

Matthew P. Woods, Preshit Gawade, Bing Tan, Umit S. Ozkan*

140 W. 19th Avenue, Department of Chemical and Biomolecular Engineering, The Ohio State University, Columbus, OH 43210, USA

ARTICLE INFO

Article history:
Received 28 November 2009
Received in revised form 2 March 2010
Accepted 9 March 2010
Available online 16 March 2010

Keywords:
PROX
CO oxidation
H_2 combustion
Cobalt
Ceria
CeO_2
Cobalt oxide
Co/CeO_2
Co_3O_4

ABSTRACT

A highly active CoO_x/CeO_2 nanoparticle catalyst with high surface area (78 m^2/g) has been prepared and tested in the preferential oxidation of carbon monoxide (PROX) in the presence of hydrogen. Three distinct temperature regions of catalyst activity are observed corresponding to CO oxidation, H_2 oxidation and methanation. The catalyst achieves near 100% CO conversion under a wide range of reaction conditions demonstrating peak activity near 175 °C. The catalyst is stable with time-on-stream at the temperature of highest CO conversion. The presence of H_2 decreases the CO oxidation rate, possibly due to competitive adsorption between H_2 and CO. CO oxidation and H_2 oxidation activation energies were 52 and 74 kJ/mol, respectively. Raman spectroscopy and X-ray diffraction experiments have demonstrated that the cobalt takes the form of Co_3O_4 and no CoO was detected under any experimental conditions.

1. Introduction

Proton exchange membrane (PEM) fuel cells have attracted significant interest due to their low temperature of operation (80 °C), high power density, high efficiency and the environmentally benign nature of their exhaust. PEM fuel cells promise to be clean and efficient alternatives to combustion of fuels for power generation in stationary and mobile applications [1,2]. Syngas can be produced from a diverse collection of domestic resources including biomass, coal and natural gas using steam reforming. The syngas then undergoes high temperature and low-temperature water gas shift reactions and the effluent, though predominantly hydrogen, may still contain 0.5–2% CO. Unfortunately, the platinum anode materials used in PEM fuel cells are easily poisoned by trace amounts of carbon monoxide. It is estimated that CO concentrations must be reduced to less than 10 ppm for a Pt anode and less than 100 ppm for CO tolerant alloy anodes [3–5]. Therefore, it is necessary to ensure that hydrogen gas fed to a fuel cell has been adequately treated to remove carbon monoxide.

One particularly attractive method of CO removal is the preferential oxidation (PROX) of carbon monoxide in hydrogen rich streams. This technique offers the benefits of low cost and ease of implementation without excessive loss of hydrogen fuel [1]. The challenge in the PROX reaction is to find catalysts that are active and selective in the appropriate temperature window. The loss of hydrogen due to undesired H_2 combustion and methanation can occur under certain conditions. Ideally, the catalyst should operate at a temperature between that of the low-temperature water gas shift reactor (250 °C) and the PEM fuel cell (~80 °C). In this temperature window, catalysts must be active for the CO oxidation reaction and inactive for the undesired side reactions.

Despite their high costs, noble metal catalysts are by far the most studied catalysts in the CO oxidation literature. Early work using the PROX reaction was performed to purify hydrogen feed streams for the production of ammonia using supported platinum, rhenium and ruthenium catalysts [6]. Some of the first PROX research to be published specifically in regard to purifying PEM feed streams was conducted by Oh and Sinkevitch [7]. They reported high activity for Ru/Al_2O_3 catalysts and high selectivities for both Ru/Al_2O_3 and Rh/Al_2O_3. Other early work investigated catalysts consisting of platinum supported on zeolites, which showed good activity and selectivity [8,9]. Other studies have demonstrated gains in activity due to the promotional effects of Fe and Co on alumina supported platinum catalysts [10–12]. At low temperatures, supported gold catalysts have been shown to be quite active, however the selectivity quickly decreases as temperature is increased [13]. For both platinum and gold catalysts, it has been proposed that H_2 and CO compete for adsorption sites on the metal atoms [14,15]. In general, platinum is considered more active than gold, but gold tends to have higher O_2 selectivity to CO_2 at low temperatures.

* Corresponding author. Tel.: +1 614 292 6623; fax: +1 614 292 3769.
E-mail address: ozkan.1@osu.edu (U.S. Ozkan).

0926-3373/$ – see front matter © 2010 Elsevier B.V. All rights reserved.
doi:10.1016/j.apcatb.2010.03.015

However, the cost and availability of the precious metal used in these catalysts is a concern.

CO oxidation studies in the absence of hydrogen and using non-precious metal catalysts have also been performed. Bulk cobalt (Co_3O_4) has been tested and shows good carbon monoxide oxidation activity. Research suggests that Co^{3+} is the active site and provides its oxygen to the carbon monoxide ultimately forming a Co^{2+} site that is re-oxidized with oxygen [16,17]. Unfortunately, Co_3O_4 catalysts deactivate with time forming Co^{2+} sites that do not re-oxidize [16]. The active Co^{3+} sites can only be recovered by high temperature treatments, usually in oxygen.

Bulk cobalt oxide has also been compared to other transition metals during preferential CO oxidation in the presence of hydrogen and has shown the highest activity [18]. Studies using bulk Co_3O_4 indicate that cobalt oxide is quite active for CO oxidation but in the excess hydrogen present under PROX reaction conditions, bulk cobalt oxide can reduce to lower valencies including metallic cobalt [19,20]. Metallic cobalt is not active for CO oxidation and has the tendency to catalyze the methanation and hydrogen combustion reactions. It is possible that, if supported on an oxide, a cobalt catalyst could be stable in a hydrogen atmosphere and retain the benefit of high activity. Previous research has shown that supported cobalt catalysts can be quite active for the PROX reaction [21]. These studies indicated that PROX activity on a Co/CeO_2 catalyst was high despite a relatively low surface area (~7 m^2/g). In the present work, a high surface area Co/CeO_2 catalyst has been prepared, characterized and tested for activity in the preferential oxidation of carbon monoxide.

2. Experimental

2.1. Catalyst synthesis

Nanoparticle CeO_2 support was prepared by dissolving $Ce(NO_3)_3{\cdot}6H_2O$ in an equal volume mixture of ethylene glycol and water to form a solution "*A*". Tert-butylamine ($(CH_3)_3CNH_2$) was dissolved in an equal volume mixture of ethylene glycol and water to form the solution "*B*". Solution *B* was added to solution *A* dropwise and the resulting solution was stirred for 15 min. This solution was then transferred to a Pyrex glass bottle, sealed and placed in a drying oven set at 100 °C for 30 h. CeO_2 precipitates were washed three times with de-ionized water and collected by vacuum filtration between each wash. The resulting precipitate was then dried in air at 100 °C overnight. The sample was calcined in air at 400 °C for 4 h with a heating rate of 10 °C/min. The resulting CeO_2 support had a BET surface area of 95 m^2/g and a pore volume of 0.21 cm^3/g as calculated using the BJH adsorption pore distribution.

Incipient wetness impregnation was used to synthesize a 10 wt% cobalt on CeO_2 catalyst. An aqueous solution of cobalt nitrate precursor, $Co(NO_3)_2{\cdot}6H_2O$ (Aldrich), was used to impregnate the previously prepared CeO_2 support. Two impregnation steps were performed on the catalyst, with a 4 h, 110 °C drying period between impregnations. After the second impregnation, the catalyst was dried at 110 °C overnight. The sample was then transferred to a calcination furnace and heated in air at a rate of 10 °C/min to 400 °C and held at that temperature for three hours.

2.2. Catalyst characterization

Static surface area and pore volume measurements were made using a Micromeritics ASAP 2010 accelerated surface area and porosimetry instrument. Experiments were conducted using nitrogen as the adsorbent at liquid nitrogen temperature (77 K). Samples were degassed under vacuum at 200 °C overnight before being analyzed. Cobalt metal dispersion was measured by hydrogen chemisorption using the static volumetric technique in a Micromeritics ASAP 2010 instrument. Catalyst pre-reduction was carried out in 100%H_2 at 500 °C for 60 min. Samples were then flushed with helium at 500 °C for 30 min before being evacuated at 510 °C. After evacuation, samples were cooled to 100 °C under vacuum before chemisorption analysis was performed using a 100%H_2 atmosphere.

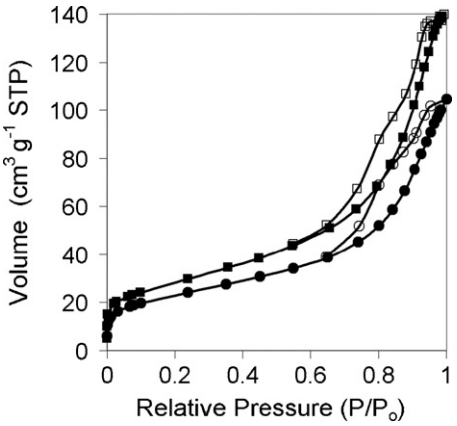

Fig. 1. Nitrogen adsorption/desorption isotherms for (■/□) CeO_2 support and (●/○) 10%CoO_x/CeO_2.

Temperature-programmed reaction (TP-Rxn) experiments were conducted to determine qualitatively the activity and selectivity of the catalyst over a wide temperature range. These experiments, described previously [22], are useful for covering a wide range of temperatures and observing where different reactions light-off. In these experiments the temperature was ramped to 350 °C at 5 °C/min rather than to 300 °C as previously published.

Transmission electron microscopy (TEM) was performed using a Phillips Tecnai F20 instrument with FEG. The instrument was operated at an accelerating voltage of 200 kV and all images were collected in bright field mode. Samples were dispersed in ethanol before being loaded onto lacey carbon copper grid.

Laser Raman spectra (LRS) were acquired using a Horiba-Jobin Yvon LabRam HR confocal Raman spectrometer as described previously [23]. Spectra were collected under atmospheric conditions on calcined Co_3O_4, CeO_2 and 10%Co/CeO_2 with a power of less than 5 mW at the sample. X-ray diffraction (XRD) experiments were performed using a Bruker D8 Advanced X-Ray Power Diffractometer with a monochromatically isolated Cu $K_{\alpha 1}$ radiation source and a Braun position sensitive detector (operated at 50 mA and 40 kV) that measures a 2θ range of 8° simultaneously. Diffraction patterns were collected in air at ambient conditions in reflection mode using a rotating 9-sample holder with polyethylene sample holders. Patterns were collected from 20° to 90° 2θ using a step size of 0.01445° and a dwell time of 1 s.

2.3. Steady-state reaction experiments

Steady-state activity measurements were performed using a reactor system and sample pre-treatment described previously [22]. Feed and effluent composition analyses were conducted using an Agilent 3000A micro gas chromatograph equipped with 0.32 mm PLOT molesieve and 0.32 mm PLOT Q columns with backflush and variable volume injectors, respectively. Both columns have TCD detectors and the detector on the mole sieve column is capable of detecting less than 5 ppm carbon monoxide. G.C. data points were collected and averaged after 60 min on stream and all carbon balances close with ±5%. The conversions of CO (X_{CO}) and O_2 (X_{O2}) as

well as the O_2 selectivity to CO_2 have been described previously [22].

Steady-state PROX experiments were conducted to test the effects of weight hourly space velocity (WHSV), O_2 and H_2 concentration and catalyst time-on-stream. Weight hourly space velocities were altered by changing the catalyst weight loaded into the reactor from 100 to 200 mg and by changing the total reactant flow rate from 50 to 25 ml/min. Weight hourly space velocities of 7500, 15,000 and 30,000 $cm^3\ g(cat)^{-1}\ h^{-1}$ were tested in the PROX reaction using 1%CO, 1%O_2, 10%H_2 and balance helium. For experiments testing the CO/O_2 concentration ratios, 1%CO and either 1% or 0.5%O_2 were tested at a WHSV of 15,000 $cm^3\ g(cat)^{-1}\ h^{-1}$. The effects of H_2 concentration were investigated using 1%CO, 2%O_2, various H_2 concentrations and balance helium at a WHSV of 30,000 $cm^3\ g(cat)^{-1}\ h^{-1}$. Time on stream reaction experiments were performed using 200 mg of 10%CoO_x/CeO_2 catalyst under a 50 ml/min flow rate of 1% CO, 1% O_2, 60% H_2 in balance helium at 175 °C. Additionally, the extent of reverse water gas shift (RWGS) over 10%CoO_x/CeO_2 catalyst was investigated in the presence of 1%CO_2, 60%H_2 and balance He at a WHSV of 30,000 $cm^3\ g(cat)^{-1}\ h^{-1}$.

CO oxidation and H_2 oxidation reactions were run using 50 mg of 10%CoO_x/CeO_2 catalyst. During CO oxidation, 3.3%CO, 3.3%O_2 and balance helium were fed over the catalyst at a flow rate of 150 ml/min at various temperatures. During H_2 oxidation, 3.3%H_2, 3.3%O_2 and balance argon were fed over the catalyst at 75 ml/min at various temperatures. CO, H_2 and O_2 conversions were limited to ensure differential reactor operation. In order to maintain isothermal conditions, a small diameter (1/4 in.) stainless steel reactor was used to ensure rapid heat flux between the reactor contents and the reactor furnace.

3. Results and discussion

3.1. Characterization of catalyst textural properties

Nitrogen adsorption/desorption isotherms were collected on the CeO_2 support and the 10%CoO_x/CeO_2 catalyst (Fig. 1). Both adsorption isotherms are similar to type II isotherm according to the IUPAC classification [24–27] suggesting the existence of macropores (>50 nm) and micropores (<2 nm). The isotherms start to increase sharply from the relative pressure at around 0.7, suggesting the existence of mesopores (2–50 nm) [26]. The isotherm plots do not show major differences between the two samples. The total volume of nitrogen adsorbed is higher on the CeO_2 support than the 10%CoO_x/CeO_2 sample. The BET surface area of the CeO_2 support is 95 m^2/g while the surface area of the 10%Co/CeO_2 sample is 78 m^2/g. These surface areas are substantially higher than those of the CeO_2 and CoO_x/CeO_2 catalysts previously tested in the PROX reaction [21].

Transmission electron microscopy of the CeO_2 support reveals agglomerated nanoparticles (see Fig. 2a). These particles are regularly shaped polyhedra approximately 4 nm across (see Fig. 2b). The very small particles are responsible for the high surface area observed during BET analysis of the support. The pore volumes measured by nitrogen adsorption/desorption are due to the aggregation of nanoparticles. The nanoparticle aggregates possess small voids between the particles leading the adsorbate condensation and the measured pore volumes. TEM images were also taken on the 10%Co/CeO_2 sample (not shown). The images did not appear different from those of the support. Small nanoparticles were observed, but cobalt oxide could not be discerned from the CeO_2 support particles. Hydrogen chemisorption experiments conducted on the 10%Co/CeO_2 catalyst support this observation showing a cobalt dispersion of 3.4%. The previously reported 10%CoO_x/CeO_2 catalyst had a cobalt dispersion of less than 0.1% [21]. Considering the relatively high activity per surface area of the low dispersion catalyst, it is reasonable to expect that this 10%Co/CeO_2 catalyst would possess high activity for CO oxidation in the presence of hydrogen.

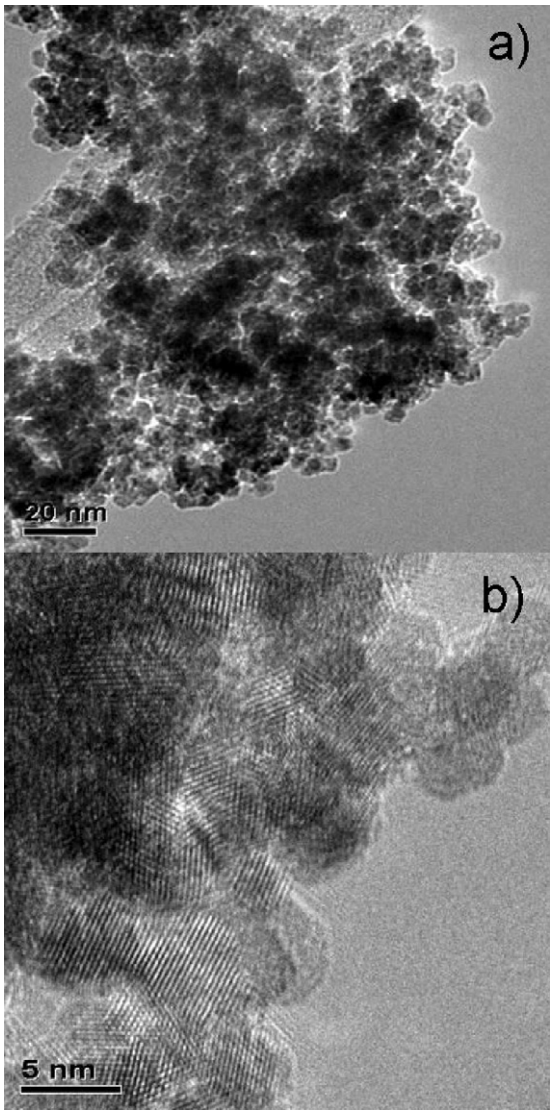

Fig. 2. TEM images of CeO_2 nanoparticles.

3.2. PROX and possible side reactions

To examine the PROX reaction network over the 10%CoO_x/CeO_2 catalyst, a temperature-programmed reaction experiment was conducted. As shown in Fig. 3, only three products were observed during the course of the experiment: CO_2, H_2O and CH_4. By following the product and reactant signals, three distinct regions of activity occurring in different temperature windows can be observed. As temperature is increased from 50 to 100 °C, the CO and O_2 signals slowly decrease while the CO_2 signal slowly increases. At 100 °C, the decrease in the CO signal becomes more substantial as does the decrease in O_2 signal and increase in CO_2 signal. At these temperatures, very little water formation is observed. The fact that the O_2 and CO signals decrease in an identical manner while the CO_2 signal appears as the mirror image of the two suggest that the predominant reaction is the selective oxidation of CO to form CO_2, though there appears to be some water forma-

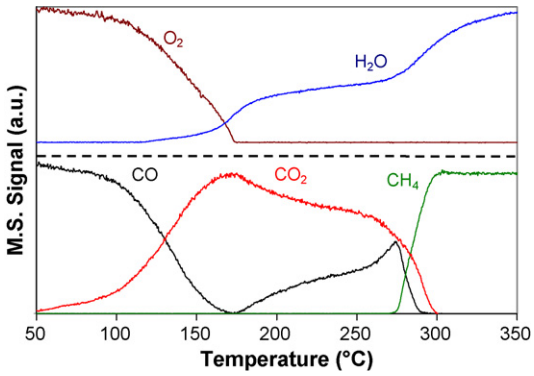

Fig. 3. Temperature-programmed PROX reaction over CoO_x/CeO_2 in the presence of 1% CO, 1% O_2, 60% H_2, balance helium.

tion. This trend continues until 175 °C is reached. As temperature is increased above 175 °C, formation of water becomes more significant and the O_2 signal reaches zero. After the O_2 signal reaches zero at 175 °C, the CO signal starts to increase while the intensity of the CO_2 signal begins to decrease. It is possible that as temperature is increased, a greater fraction of oxygen is consumed in the combustion of hydrogen. Other possible reactions include reverse water gas shift and methanation. The CO signal continues to increase until 275 °C and it should be noted that despite the competition from H_2 combustion, CO_2 is always being formed and the CO signal never reaches its initial intensity suggesting that significant CO oxidation is still occurring. Above 275 °C, however, the situation changes and the CO and CO_2 signals quickly decrease to zero. Concurrently, the methane signal increases before leveling out around 300 °C and the water signal rises at a faster rate.

In order to explore the possibility of reverse water gas shift reaction over 10%CoO_x/CeO_2 catalyst, especially in the temperature range of 175–275 °C, a steady-state reaction experiment was performed using a feed stream of 1%CO_2 and 60% H_2. Fig. 4 shows the CO_2 conversion as a function of temperature, with the inset showing the CO_2 and CH_4 percent yields. CO_2 conversion was found to be minimal below 200 °C (less than 4%), suggesting the extent of reverse water gas shift reaction is negligible. Although, further increase in temperature results in a considerable increase in CO_2 conversion, reaching 66% at 275 °C, the product distribution, as shown in the Fig. 4 inset, suggests that the majority of CO_2 was converted to CH_4 rather than CO indicating that methanation was more favored than the reverse water gas shift reaction above 200 °C. These results also indicate that during the temperature-programmed PROX experiments, RWGS activity is negligible. The observed decrease in CO_2 concentration and the

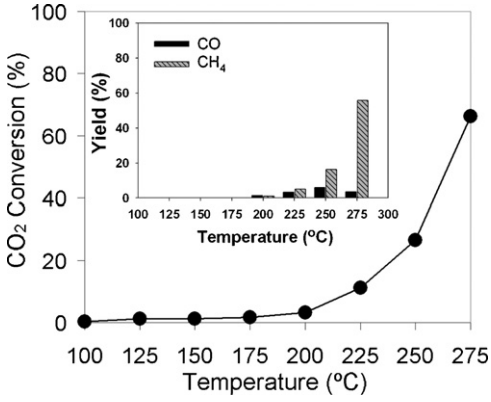

Fig. 4. (●) CO_2 conversion in reverse water gas shift. Inset shows % yield of CO and CH_4. Reaction conditions: 1%CO_2, 60%H_2, balance He, WHSV 30,000 $cm^3\ g(cat)^{-1}\ h^{-1}$.

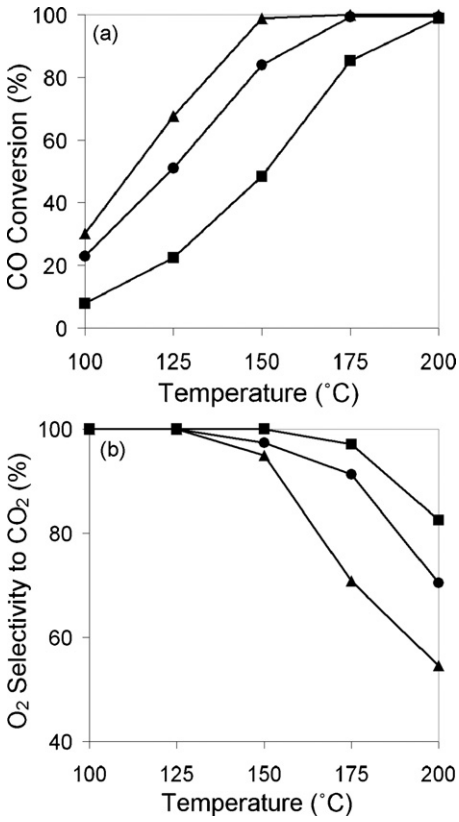

Fig. 5. (a) CO conversion and (b) O_2 selectivity to CO_2 during PROX at (▲) 7500 (●) 15,000 and (■) 30,000 $cm^3\ g(cat)^{-1}\ h^{-1}$.

concurrent increase in CO concentration starting at 175 °C is likely due to the competitive combustion of hydrogen.

3.3. Catalyst activity at various weight hourly space velocities

The steady-state activity of our CoO_x/CeO_2 catalyst was studied at three different weight hourly space velocities: 7500, 15,000 and 30,000 $cm^3\ g(cat)^{-1}\ h^{-1}$ using 1%CO, 1%O_2, 10%H_2 and balance helium. Fig. 5a shows the CO conversion at these three weight hourly space velocities. At a given temperature, increasing the weight hourly space velocity decreases the CO conversion. At 7500 $cm^3\ g(cat)^{-1}\ h^{-1}$, the CO conversion reaches near 100% at 150 °C and remains at this level as temperature is further increased. Upon increasing the WHSV to 15,000 $cm^3\ g(cat)^{-1}\ h^{-1}$, however, the temperature at which 100% CO conversion occurs increases to 175 °C. CO conversion does not change as temperature is further increased to 200 °C. As WHSV is further increased to 30,000 $cm^3\ g(cat)^{-1}\ h^{-1}$, the CO conversion decreases again reaching a maximum near 100% at 200 °C. The O_2 conversion (not shown) follows a similar trend, as expected, with higher conversions occurring at lower WHSV. These results demonstrate that the CoO_x/CeO_2 catalyst is highly active for the preferential CO oxidation reaction and under the given reaction conditions, complete CO conversion can be achieved within the desired temperature window over a range of residence times.

Fig. 5b shows the O_2 selectivity to CO_2 for the 10% CoO_x/CeO_2 catalyst using 1% CO, 1% O_2, 10% H_2 and balance helium. For all weight hourly space velocities, the selectivity drops monotonically as the temperature increases. Additionally, at all weight hourly space velocities, the O_2 selectivity to CO_2 remains at 95% or above at temperatures below 150 °C. In fact, all catalysts show near 100% selectivity at temperatures of 125 °C and below. As temperatures are increased above 150 °C, selectivity drops for all weight

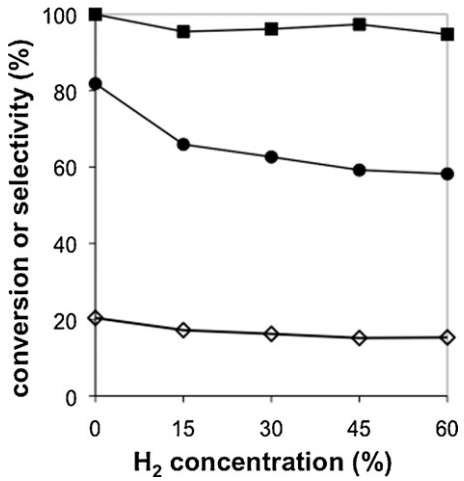

Fig. 6. (●) CO conversion and (■) O_2 selectivity to CO_2 and (◊) O_2 conversion during steady-state PROX at 150 °C over 10%Co/CeO_2 at various hydrogen concentrations. (Reaction conditions: 1%CO, 2%O_2, various hydrogen concentrations, WHSV 30,000 cm^3 $g(cat)^{-1}$ h^{-1}, T = 150 °C.)

hourly space velocities tested as the rate of hydrogen combustion increases. At 30,000 and 15,000 cm^3 $g(cat)^{-1}$ h^{-1}, selectivity at 200 °C drops to 83% and 70%, respectively. At 7500 cm^3 $g(cat)^{-1}$ h^{-1}, selectivity drops more rapidly reaching 55% at 200 °C. These results show that at a temperature 150 °C or below, the 10% CoO_x/CeO_2 catalyst is able to achieve high O_2 to CO_2 selectivities while at the same time achieving high carbon monoxide conversion. The increase in O_2 selectivity to CO_2 with increasing WHSV is due to the lesser extent of hydrogen combustion in experiments using higher space velocities.

The steady-state PROX activity of the current nano-structured CoO_x/CeO_2 formulation was compared with the previously developed CoO_x/CeO_2 (low surface area) catalyst [21] on an equal weight and on an equal BET surface area basis (not shown). In both cases, the present high surface area formulation was found to have a much higher PROX activity over the temperature range studied.

3.4. Effect of H_2 and O_2 concentrations on PROX performance over 10%CoO_x/CeO_2

Steady-state PROX experiments were conducted to determine the performance of 10%CoO_x/CeO_2 under various concentrations of hydrogen. CO conversion and O_2 selectivity to CO_2 as a function of the H_2 concentration of the feed are shown in Fig. 6. As expected, as hydrogen is introduced into the feed, the O_2 selectivity to CO_2 decreases. When 15% H_2 is introduced, the selectivity drops from 100% to 96%. As H_2 concentration is further increased, O_2 selectivity to CO_2 drops further reaching 92% when the feed contains 60% H_2. Selectivity drops with the introduction of hydrogen due to the consumption of oxygen in the hydrogen combustion reaction.

As shown in Fig. 6, the CO conversion decreases from 82% to 66% when hydrogen is introduced into the feed at a concentration of 15%. Smaller decreases in conversion continue as the feed concentration of hydrogen is increased. Ultimately a CO conversion of 58% is reached when the feed concentration of hydrogen is 60%. What is more interesting is that upon the introduction of hydrogen, the O_2 consumption rate does not increase (see Fig. 6). This suggests that CO conversion is not decreasing due to a decrease in oxygen concentration caused by the unselective H_2 combustion reaction. The decrease in CO conversion could be explained by the competitive adsorption of hydrogen on sites responsible for the PROX reaction. It has been suggested that the CO and H_2 oxidation reactions occur on independent sites on the CuO-CeO_2 [28,29] catalytic system. Our

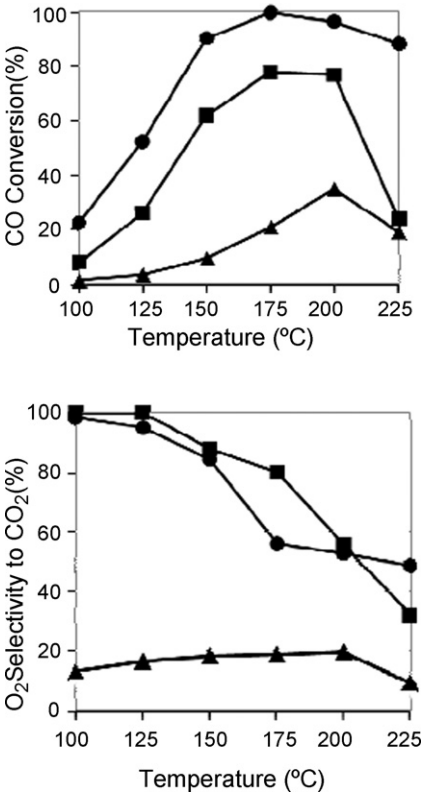

Fig. 7. (a) CO conversion (b) O_2 selectivity to CO_2 PROX during steady-state. (●) 1%O_2 over 10%Co/CeO_2 and (■) 0.5%O_2 over 10%Co/CeO_2 (▲) 1%O_2 over CeO_2 support. (Reaction conditions: 1%CO, 60% H_2, WHSV of 15,000 cm^3 $g(cat)^{-1}$ h^{-1}.)

results on the CoO_x/CeO_2 system do not preclude the existence of separate sites. The results do, however, demonstrate that hydrogen interacts with the sites responsible for both PROX and H_2 oxidation.

Steady-state PROX experiments were also conducted to determine the effect of the O_2/CO concentration ratio in the presence of high concentrations of hydrogen. In these experiments, the reactant concentrations were 1%CO, 1%O_2 or 0.5%O_2, 60%H_2 and balance helium. Additionally, the CeO_2 nanoparticle support (without any cobalt loading) was tested for preferential CO oxidation activity. Fig. 7a shows the effect of oxygen concentration on CO conversion during the steady-state PROX reaction. Over the 10%CoO_x/CeO_2 catalyst, changing from stoichiometric to excess oxygen increases the CO conversion substantially. With both excess and stoichiometric O_2 concentrations, the CO conversion rate increases with temperature until reaching a maximum at 175 °C. When using stoichiometric and excess concentrations of oxygen, the maximum CO conversions are 78% and 99.9%, respectively. At temperatures above 175 °C, the CO conversion begins to decrease due to the competitive combustion of hydrogen. When using stoichiometric oxygen (0.5% O_2), as temperature increases above 200 °C the CO conversion drops dramatically. This is due to complete consumption of all the oxygen. CO conversion over the bare CeO_2 nanoparticles follows a similar trend, though the carbon monoxide conversion is substantially lower than on the 10%CoO_x/CeO_2 catalyst. The CeO_2 reaches a maximum CO conversion of 34% at 175 °C before the activity begins to decrease due to hydrogen combustion. These results indicate that when using excess O_2, complete conversion of CO can be obtained at 175 °C under the given reaction conditions. The low CO conversion over CeO_2 indicates that the presence of cobalt is predominantly responsible for the oxidation of carbon monoxide.

Fig. 7b shows the O_2 to CO_2 selectivity during the steady-state PROX reaction. The reaction using a stoichiometric amount of oxygen has a higher selectivity at all temperatures except for 225 °C.

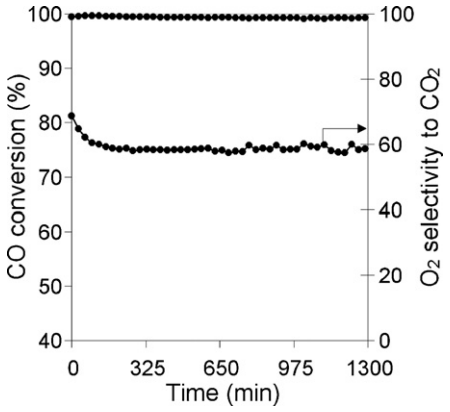

Fig. 8. Time-on-stream CO conversion and O_2 selectivity to CO_2 on CoO_x/CeO_2 at 175 °C in the presence of 1% CO, 1% O_2, and 60% H_2, balance helium at WHSV of 15,000 $cm^3\ g(cat)^{-1}\ h^{-1}$.

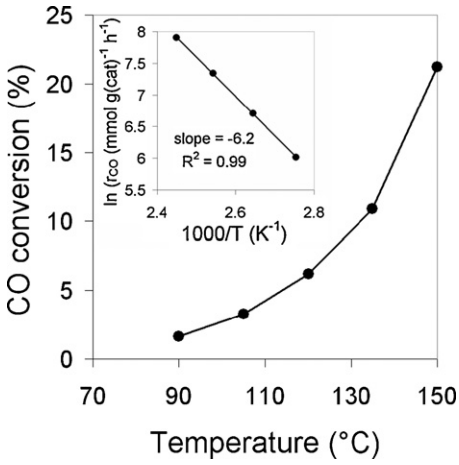

Fig. 9. CO conversion over $10\%CoO_x/CeO_2$ during steady-state carbon monoxide oxidation experiments. Reaction conditions: 3.3%CO, 3.3%O_2, balance helium. Inset–Arrhenius plot of CO oxidation activation energy.

This shows that, although the CO conversion is improved under increased oxygen concentrations, the O_2 selectivity to CO_2 actually decreases. For both excess and stoichiometric amounts of oxygen, the selectivity begins at its maximum and decreases with temperature. High selectivities can be obtained with the $10\%CoO_x/CeO_2$ catalyst when operating under certain conditions. At 150 °C under excess oxygen, we are able to obtain 85% O_2 selectivity to CO_2 at over 90% CO conversion. At 175 °C under excess oxygen, O_2 selectivity to CO_2 is still 56% while CO conversion is 99.9%. Above 225 °C the O_2 selectivity to CO_2 under stoichiometric oxygen conditions drops below that obtained under excess oxygen conditions. This is due to the complete consumption of oxygen under the stoichiometric conditions. At the temperatures used in these steady-state reactions, no methane was detected indicating the loss in selectivity is due entirely to the combustion of hydrogen in agreement with the previously presented temperature-programmed PROX experiments.

Stability has been a concern on other cobalt based catalysts and activity losses have been attributed to the reduction of CoO_x to lower valency states [18]. The stability of the catalyst under the reducing conditions of the PROX reaction is important for long term performance. In order to further characterize the stability of $10\%CoO_x/CeO_2$ under the reducing conditions of the PROX reaction, time-on-stream studies were performed. These experiments were conducted using a feed composition of 1%CO, 1%O_2 and 60%H_2 at a weight hourly space velocity of 15,000 $cm^3\ g(cat)^{-1}\ h^{-1}$ and a temperature of 175 °C. Fig. 8 shows the time-on-stream CO conversion of $10\%CoO_x/CeO_2$. No discernible decrease in activity occurs during the course of the reaction. Additionally, the O_2 selectivity to CO_2 (see Fig. 8) quickly reaches 58% and remains stable over the course of the time-on-stream experiment. These results suggest that on this particular catalyst, reduction of Co_3O_4 to lower valency states may not be occurring. Previous research has demonstrated that bulk reduction of Co^{3+} in supported cobalt catalyst does not occur until temperatures higher than 175 °C [22].

3.5. CO and H_2 oxidation on 10% CoO_x/CeO_2

Insight into the PROX reaction network can be gained by separately studying the oxidation of CO and H_2. By running separate reactions, the kinetic parameters of each can be determined and compared to the reaction results where both reactants are co-fed over the catalyst. CO and H_2 oxidation experiments were independently performed over $10\%CoO_x/CeO_2$ catalyst to investigate the two reaction pathways. CO oxidation was carried out using 3.3%CO, 3.3%O_2 and balance helium. Fig. 9 shows the CO conversion as a function of temperature. CO conversion increases monotonically with temperature until reaching 21% at 150 °C. The activation energy for CO oxidation was calculated using the four points collected at the four lowest temperatures to keep CO conversions below 15%. The Fig. 9 inset shows the Arrhenius plot for CO oxidation. The resulting slope is −6.2 which corresponds to a CO oxidation activation energy of 52 kJ/mol over our $10\%CoO_x/CeO_2$ catalyst. Similar results have been reported previously over a cobalt on zirconia catalyst [23].

H_2 oxidation was carried out using 3.3%H_2, 3.3%O_2 and balance argon. The H_2 conversion as a function of temperature is presented in Fig. 10. Measurable H_2 conversions are only obtainable at temperatures higher than those used in the CO oxidation experiments. An H_2 conversion of 1.6% is obtained at 150 °C and increases monotonically until reaching 22% at 210 °C. The activation energy for H_2 oxidation was calculated using the four points collected at the four lowest temperatures. The Fig. 10 inset shows the Arrhenius plot for H_2 oxidation. The resulting slope is −8.9 which corresponds to an H_2 oxidation activation energy of 74 kJ/mol on 10% CoO_x/CeO_2. The higher activation energy of H_2 oxidation accounts for the temperature-programmed PROX results (Fig. 3) showing that hydrogen oxidation is more temperature-sensitive and becomes important above 175 °C. The fact that H_2 oxidation is not dominant at lower temperatures is due to the higher activation energy of the reaction for H_2 oxidation. This difference results

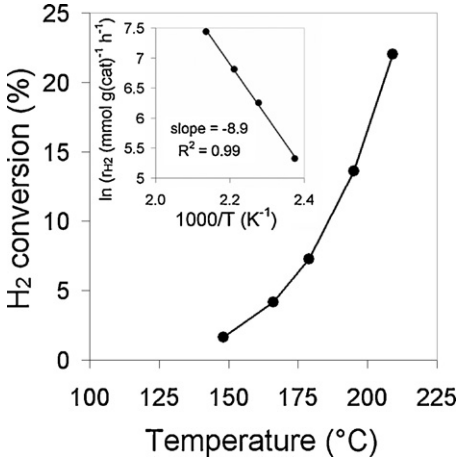

Fig. 10. H_2 conversion over $10\%CoO_x/CeO_2$ during steady-state hydrogen oxidation experiments. Reaction conditions: 3.3%H_2, 3.3%O_2, balance helium. Inset–Arrhenius plot of H_2 oxidation activation energy.

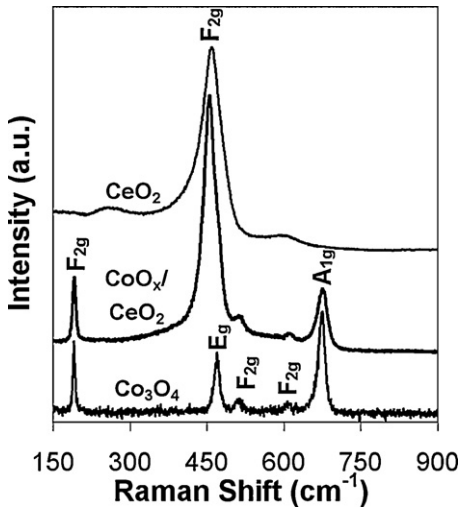

Fig. 11. Raman spectra of CeO_2, Co_3O_4 and CoO_x/CeO_2.

in the requirement for optimum temperatures high enough for CO oxidation activity, but not too high such that H_2 oxidation reaction is able to occur at appreciable rates.

3.6. Structural properties of 10% CoO_x/CeO_2

Fig. 11 shows Raman spectra collected using the 633 nm line for Co_3O_4, CoO_x/CeO_2 and CeO_2 nanoparticles. The Co_3O_4 spectra shows five active Raman modes typical of the spinel structure located at 193, 475, 516, 615 and 680 cm^{-1}. The peaks at 193, 516 and 615 cm^{-1} have been attributed to the F_{2g} phonon mode while the peaks at 475 and 680 cm^{-1} have been assigned to the E_g and A_{1g} phonon modes, respectively [30,31]. The Raman spectrum of CeO_2 shows a single broad and intense band located at 462 cm^{-1}. This peak is assigned to the F_{2g} phonon mode of cubic fluorite CeO_2 [32–34]. The Raman spectrum of CoO_x/CeO_2 clearly shows peaks characteristic of Co_3O_4 located at 193 and 615 cm^{-1}. Additionally, there are two overlapping peaks located at 459 and 472 cm^{-1}. The peak at 459 cm^{-1} is assigned to the F_{2g} phonon mode of CeO_2 while the peak at 472 cm^{-1} is assigned to the E_g phonon mode of Co_3O_4. The presence of peaks at 193, 472 and 615 cm^{-1} indicate that cobalt is present as Co_3O_4. A spectrum was also collected from spent Co/CeO_2 after the PROX reaction (not shown). The spent catalyst spectrum only shows the peaks present in the fresh sample indicating that CeO_2 and Co_3O_4 have not been substantially reduced during reaction.

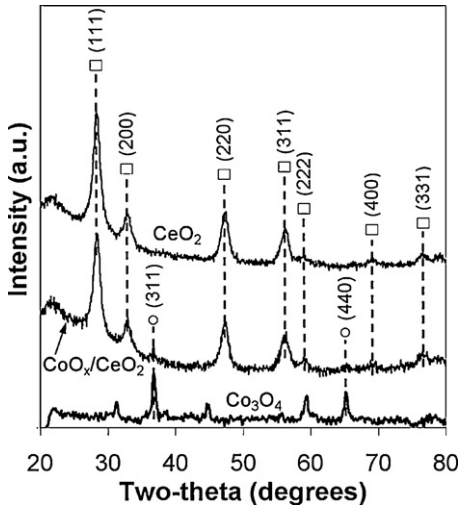

Fig. 12. X-ray diffraction patterns of CeO_2, Co_3O_4 and CoO_x/CeO_2, where (○): Co_3O_4 and (□): CeO_2 cubic fluorite.

X-ray diffraction patterns were collected for lab-synthesized Co_3O_4, CeO_2 and CoO_x/CeO_2 samples and are shown in Fig. 12. The Co_3O_4 used as a reference, show diffraction peaks characteristic of the spinel structure with the (2 2 0), (3 1 1), (4 0 0), (5 1 1) and (4 4 0) reflections occurring at 31.3°, 36.8°, 44.9°, 59.4° and 65.3° 2θ, respectively [35]. The XRD pattern for the CeO_2 nanoparticles is typical of the cubic fluorite structure with peaks at 28.2°, 33.0°, 47.5°, 56.5°, 59.3° 69.3° and 76.8° 2θ representing the (1 1 1), (2 0 0), (2 2 0), (3 1 1), (2 2 2), (4 0 0) and (3 3 1) reflections, respectively [36].

The 10%CoO_x/CeO_2 diffraction pattern shows strong diffraction lines due to CeO_2 and weaker ones due to Co_3O_4. The (1 1 1), (2 0 0), (2 2 0), (3 1 1), (4 0 0) and (3 1 1) peaks of CeO_2 are all present. There is also a small peak present at 59.3° which is assigned to the (2 2 2) reflection of CeO_2 though it should be noted that Co_3O_4 gives a peak at 59.4° 2θ. Regardless of the identity of this peak, there are two peaks that can be unambiguously attributed to the presence of Co_3O_4 on the CoO_x/CeO_2 sample. These peaks, present due to the (3 1 1) and (4 4 0) reflections of Co_3O_4, are located at 36.8° and 65.3° 2θ, respectively.

It should be noted that no evidence of CoO was observed in the Raman spectrum of fresh or spent catalysts or the XRD pattern of the fresh CoO_x/CeO_2 catalyst. CoO peaks, which are not observed, would be located at 143, 221 and 296 cm^{-1} [37] in Raman spectroscopy and 36.9°, 42.9°, 62.0°, 73.3° and 77.4° 2θ [38] in X-ray diffraction experiments. These results show that crystalline Co_3O_4 is formed on the CeO_2 support during calcinations at 400 °C in air. It is not surprising that Co_3O_4 is detected rather than CoO due to the higher thermodynamic stability of Co_3O_4 [39] both under ambient conditions and at higher temperatures.

4. Conclusions

This work demonstrates the preparation of a high-surface area 10%CoO_x/CeO_2 catalyst that is highly effective for the preferential oxidation of carbon monoxide in a hydrogen rich feed. Results indicate a mesoporous, nanoparticle CeO_2 support a CoO_x/CeO_2 catalyst with a surface area of 78 m^2/g. The dispersion and surface area of this catalyst are far superior to those of a previously tested CoO_x/CeO_2 catalyst [21]. Raman spectroscopy and X-ray diffraction experiments have demonstrated that the cobalt takes the form of Co_3O_4 and no CoO was detected under any experimental conditions. It is possible that the octahedral Co^{3+} sites are the active sites for oxidation of carbon monoxide [40].

Three distinct temperatures regions of catalyst activity occur. Below 175 °C CO oxidation is dominant. Between 175 and 275 °C, CO oxidation competes with H_2 combustion. Above 275 °C, methanation dominates. The 10%CoO_x/CeO_2 catalyst is able to achieve near 100% CO conversion under a wide range of conditions depending on WHSV and O_2 concentration. This catalyst is stable with time-on-stream at the temperature of highest CO conversion. H_2 concentration seems to have a negative effect on the CO oxidation rate and O_2 to CO_2 selectivity decreases suggesting that H_2 competes with CO for adsorption sites. CO oxidation and H_2 oxidation activation energies were 52 and 74 kJ/mol, respectively over the 10%Co/CeO_2 catalyst, which accounts for the increasing importance of H_2 oxidation at higher temperatures.

Acknowledgements

The financial support provided for this work by the Ohio Coal Development Office, the Ohio Department of Development through the Wright Center of Innovation and U.S. Department of Energy

through the grant DE-FG36-05GO15033 is gratefully acknowledged.

References

[1] A. Faur Ghenciu, Current Opinion in Solid State & Materials Science 6 (2002) 389–399.
[2] B.C.H. Steele, A. Heinzel, Nature (London, United Kingdom) 414 (2001) 345–352.
[3] J.L. Ayastuy, M.A. Gutierrez-Ortiz, J.A. Gonzalez-Marcos, A. Aranzabal, J.R. Gonzalez-Velasco, Industrial & Engineering Chemistry Research 44 (2005) 41–50.
[4] L. Shore, R. J. Farrauto, In: W. Vielstich, A. Lamm, H. Gasteiger, (Eds.), *Handbook of Fuel Cells: Fundamentals Technology and Applications*, John Wiley and Sons Ltd, Chichester, England, Vol. 3, Part 1, 211–212, 2003.
[5] D.L. Trimm, Z.I. Onsan, Catalysis Reviews - Science and Engineering 43 (2001) 31–84.
[6] M.L. Brown Jr., A.W. Green, G. Cohn, H.C. Andersen, Journal of Industrial and Engineering Chemistry (Washington, D.C.) 52 (1960) 841–844.
[7] S.H. Oh, R.M. Sinkevitch, Journal of Catalysis 142 (1993) 254–262.
[8] H. Igarashi, H. Uchida, M. Suzuki, Y. Sasaki, M. Watanabe, Applied Catalysis, A: General 159 (1997) 159–169.
[9] I. Rosso, C. Galletti, S. Fiorot, G. Saracco, E. Garrone, V. Specchia, Journal of Porous Materials 14 (2007) 245–250.
[10] B.-K. Chang, Y. Lu, B.J. Tatarchuk, Chemical Engineering Journal (Amsterdam, Netherlands) 115 (2006) 195–202.
[11] G.W. Roberts, P. Chin, X. Sun, J.J. Spivey, Applied Catalysis, B: Environmental 46 (2003) 601–611.
[12] M. Watanabe, H. Uchida, K. Ohkubo, H. Igarashi, Applied Catalysis, B: Environmental 46 (2003) 595–600.
[13] S. Kandoi, A.A. Gokhale, L.C. Grabow, J.A. Dumesic, M. Mavrikakis, Catalysis Letters 93 (2004) 93–100.
[14] M.M. Schubert, V. Plzak, J. Garche, R.J. Behm, Catalysis Letters 76 (2001) 143–150.
[15] B. Schumacher, Y. Denkwitz, V. Plzak, M. Kinne, R.J. Behm, Journal of Catalysis 224 (2004) 449–462.
[16] J. Jansson, A.E.C. Palmqvist, E. Fridell, M. Skoglundh, L. Oesterlund, P. Thormaehlen, V. Langer, Journal of Catalysis 211 (2002) 387–397.
[17] P. Broqvist, I. Panas, H. Persson, Journal of Catalysis 210 (2002) 198–206.
[18] Y. Teng, H. Sakurai, A. Ueda, T. Kobayashi, International Journal of Hydrogen Energy 24 (1999) 355–358.
[19] K. Omata, Y. Kobayashi, M. Yamada, Catalysis Communications 6 (2005) 563–567.
[20] S. Ozkara, A.N. Akin, Z. Misirli, A.E. Aksoylu, Turkish Journal of Chemistry 29 (2005) 219–224.
[21] Z. Zhao, M.M. Yung, U.S. Ozkan, Catalysis Communications 9 (2008) 1465–1471.
[22] M.M. Yung, Z. Zhao, M.P. Woods, U.S. Ozkan, Journal of Molecular Catalysis A: Chemical 279 (2008) 1–9.
[23] M.M. Yung, E.M. Holmgreen, U.S. Ozkan, Catalysis Letters 118 (2007) 180–186.
[24] S. Chen, X. Zhang, P. Shen, Electrochemistry Communications 8 (2006) 713.
[25] K.S.W. Sing, Pure and Applied Chemistry 54 (1982) 2201–2218.
[26] B. Holland, Journal of Porous Materials 10 (2003) 17–22.
[27] K.S.W. Sing, R.A. Haul, R.A. Pierotti, T. Siemieniewska, Pure and Applied Chemistry 57 (1985) 603–619.
[28] H.C. Lee, D.H. Kim, Catalysis Today 132 (2008) 109–116.
[29] M.M. Schubert, M.J. Kahlich, H.A. Gasteiger, R.J. Behm, Journal of Power Sources 84 (1999) 175–182.
[30] J. Jiang, L. Li, Materials Letters 61 (2007) 4894–4896.
[31] V. Khadzhiev, M. Iliev, I. Vergilov, Journal of Physics C: Solid State Physics 21 (1988) L199–L201.
[32] V.G. Keramides, W.B. White, Journal of Chemical Physics 59 (1973) 1561–1562.
[33] R. Kostic, S. Askrabic, Z. Dohcevic-Mitrovic, Z.V. Popovic, Applied Physics A: Materials Science & Processing 90 (2008) 679–683.
[34] Z.V. Popovic, Z. Dohcevic-Mitrovic, A. Cros, A. Cantarero, Journal of Physics: Condensed Matter 19 (2007) 496209/496201-496209/496209.
[35] P. Dutta, M.S. Seehra, S. Thota, J. Kumar, Journal of Physics: Condensed Matter 20 (2008) 015218/015211-015218/015218.
[36] C. Pan, D. Zhang, L. Shi, Journal of Solid State Chemistry 181 (2008) 1298–1306.
[37] H.H. Chou, H.Y. Fan, Physical Review B: Solid State 13 (1976) 3924–3938.
[38] Y. Zhang, X. Zhong, J. Zhu, X. Song, Nanotechnology 18 (2007) 195605/195601-195605/195605.
[39] S.C. Petitto, E.M. Marsh, G.A. Carson, M.A. Langell, Journal of Molecular Catalysis A: Chemical 281 (2008) 49–58.
[40] K. Omata, T. Takada, S. Kasahara, M. Yamada, Applied Catalysis A: General 146 (1996) 255–267.